AIAA 93-2906
Zonal Two Equation k-ω Turbulence Models for Aerodynamic Flows.

Florian R. Menter
Eloret Institute, Sunnyvale.
Mailing Address:
NASA-Ames Research Center, MS 229-1,
Moffett Field CA. 94035-1000.

24th Fluid Dynamics Conference
July 6-9, 1993 / Orlando, Florida

ZONAL TWO EQUATION k-ω TURBULENCE MODELS FOR AERODYNAMIC FLOWS

F. R. Menter
Eloret Institute
Sunnyvale, CA

Abstract

Two new versions of the $k-\omega$ two-equation turbulence model will be presented. The new Baseline (BSL) model is designed to give results similar to those of the original $k-\omega$ model of Wilcox, but without its strong dependency on arbitrary freestream values. The BSL model is identical to the Wilcox model in the inner 50% of the boundary-layer but changes gradually to the standard $k-\epsilon$ model (in a $k-\omega$ formulation) towards the boundary-layer edge. The new model is also virtually identical to the $k-\epsilon$ model for free shear layers. The second version of the model is called Shear-Stress Transport (SST) model. It is a variation of the BSL model with the additional ability to account for the transport of the principal turbulent shear stress in adverse pressure gradient boundary-layers. The model is based on Bradshaw's assumption that the principal shear-stress is proportional to the turbulent kinetic energy, which is introduced into the definition of the eddy-viscosity. Both models are tested for a large number of different flowfields. The results of the BSL model are similar to those of the original $k-\omega$ model, but without the undesirable freestream dependency. The predictions of the SST model are also independent of the freestream values but show better agreement with experimental data for adverse pressure gradient boundary-layer flows.

Introduction

The main field of application of Navier-Stokes methods in aerodynamics will be for complex turbulent flows that cannot be treated by inviscid, or viscous-inviscid interaction schemes. Examples are massively separated flows, flows involving multiple length-scales, flows with three-dimensional separation and complex unsteady flows. In these flows, the application of algebraic turbulence models, like the Cebeci-Smith [1], the Baldwin-Lomax [2] or the Johnson-King [3] model, becomes very complicated and often ambiguous, mainly because of the difficulty to define an algebraic length-scale. It is obvious that the improvement of numerical methods must be accompanied by the development of more general turbulence models and their implementation into Navier-Stokes codes.

In addition to being independent of the specification of an algebraic length-scale, there is a long list of characteristics a good turbulence model would have to satisfy. Obviously, the model should be "sufficiently" accurate for the intended type of applications. Furthermore, and almost as important, the model must be numerically robust and should not consume excessive amounts of computation time (compared to the mean-flow solver). Another important demand is that the results should not have a strong dependency on ambiguous quantities, especially on the specified freestream values.

The most popular non-algebraic turbulence models are two-equation eddy-viscosity models. These models solve two transport equations, generally one for the turbulent kinetic energy and another one related to the turbulent length- (or time-) scale. Among the two-equation models, the $k-\epsilon$ model is by far the most widely used today. The first low Reynolds number $k-,\epsilon$ model was developed by Jones and Launder [4] and has subsequently been modified by many authors.

The $k-\epsilon$ model has been very successful in a large variety of different flow situations, but it also has a number of well known shortcomings. From the standpoint of aerodynamics, the most disturbing is the lack of sensitivity to adverse pressure-gradients. Under those conditions, the model significantly overpredicts the shear-stress levels and

AIAA 24th Fluid Dynamics Conference, July 6-9, 1993, Orlando, Florida

thereby delays (or completely prevents) separation [5]. Rodi [6] attributes this shortcoming to the overprediction of the turbulent length-scale in the near wall region and has shown that a correction proposed by Hanjalic and Launder improves the predictions considerably. However, the correction is not coordinate-invariant and can therefore not be applied generally. An alternative way of improving the results has been proposed by Chen and Patel [7] and by Rodi [8]. They replace the ϵ-equation in the near wall region by a relation that specifies the length-scale analytically. This also reduces some of the stiffness problems associated with the solution of the model. Although the procedure is coordinate independent, it has only been applied to relatively simple geometries, where the change between the algebraic relation and the ϵ - equation could be performed along a pre-selected gridline. Clearly this cannot be done in flows around complex geometries. Furthermore, the switch has to be performed in the logarithmic part (the algebraic length-scale is not known in the wake region), so that the original $k-\epsilon$ model is still being used over most of the boundary layer.

Another shortcoming of the $k-\epsilon$ model is associated with the numerical stiffness of the equations when integrated through the viscous sublayer. This problem clearly depends on the specific version of the $k-\epsilon$ model selected, but there are some general aspects to it. All low Reynolds number $k-\epsilon$ models employ damping functions in one form or another in the sublayer. These are generally nonlinear functions of dimensionless groups of the dependent variables like $R_t = \frac{k^2}{\epsilon\nu}$. The behavior of these functions cannot easily be controlled by conventional linearization techniques and can therefore interfere with the convergence properties of the scheme. A second problem is that ϵ does not go to zero at a no-slip surface. That in turn leaves two alternatives. One is to employ a nonlinear boundary condition on ϵ ($\epsilon = f(\frac{\partial\sqrt{k}}{\partial y})$), or to add additional terms to the ϵ - equation [4] that allow the use of a homogeneous boundary condition. Both approaches introduce additional nonlinearities that can upset a numerical procedure.

There is a significant number of alternative models [9, 10, 11] that have been developed to overcome the shortcomings of the $k-\epsilon$ model. One of the most successful, with respect to both, accuracy and robustness, is the $k-\omega$ model of Wilcox [9]. It solves one equation for the turbulent kinetic energy k and a second equation for the specific turbulent dissipation rate (or turbulence frequency) ω. The model performs significantly better under adverse pressure-gradient conditions than the $k-\epsilon$ model although it is the author's experience that an even higher sensitivity to strong adverse pressure-gradients would be desirable [12]. Another strongpoint of the model is the simplicity of its formulation in the viscous sublayer. The model does not employ damping functions and has straightforward Dirichlet boundary conditions. This leads to significant advantages in numerical stability.

However, the $k-\omega$ model also has a major shortcoming. It has been reported recently that the results of the model depend strongly on the freestream values, ω_f, that are specified outside the shear-layer. In [13] this problem has been investigated in detail, and it has been shown that the magnitude of the eddy-viscosity can be changed by more than 100% just by using different values for ω_f. This is clearly unacceptable and corrections are necessary to ensure unambiguous solutions.

In this paper, two new turbulence models will be presented. First, a new baseline (BSL) $k-\omega$ model will be described. It is identical to the $k-\omega$ model of Wilcox [9] for the inner region of a boundary layer (up to approximately $\delta/2$) and gradually changes to the standard $k-\epsilon$ model in the outer wake region. In order to be able to perform the computations with one set of equations, the $k-\epsilon$ model was first transformed into a $k-\omega$ formulation. The blending between the two regions is performed by a blending function F_1 that gradually changes from one to zero in the desired region. No a priori knowledge of the flowfield is necessary to perform the blending. The function also ensures that the $k-\epsilon$ formulation is selected for free shear-layers. The performance of the new (BSL) model is very similar to that of the Wilcox $k-\omega$ model for adverse pressure gradient boundary-layer flows (and therefore significantly better than that of the $k-\epsilon$ model), but without the undesirable freestream dependency. For free shear layers the new model is basically identical to the $k-\epsilon$ model, which predicts spreading rates more accurately than the $k-\omega$ model.

Although the original - and the new BSL $k-\omega$ model perform better in adverse pressure gradient flows than the $k-\epsilon$ model, they still underpredict the amount of separation for severe adverse pressure gradient flows [12]. In an attempt to improve matters, the eddy-vicosity formulation of the BSL model will be modified to account for the transport effects of the principal turbulent shear-stress. The motivation for this modification comes from the Johnson-King (JK) model [3] which has proven to be highly successful for adverse pressure gradient flows. The JK-model is based on the assumption that the turbulent shear-stress is proportional to the turbulent kinetic energy in the logarithmic and wake regions of a turbulent boundary layer. Johnson and King solve an equation for the maximum turbulent shear-stress at each downstream station and limit the eddy-viscosity in order to satisfy this proportionality. In the framework of two-equation models the turbulent kinetic energy is already known and it is therefore only necessary to limit the eddy-viscosity to account for the same effect. The resulting model will be called shear-stress transport (SST) model. First predictions based on this assumption have already been reported in [12].

The BSL and the SST models are not significantly more complicated than the original $k-\omega$ model and consume only little more computing time. Because the two models are virtually identical to the original $k-\omega$ model in the near wall

region, the modifications developed by Wilcox [9] for rough walls and for surface mass injection can be applied without changes. Furthermore, the models have shown the same numerical robustness as the original model for all the flows computed so far. The present paper is based on the work presented in [14]. However the equations have been changed somewhat in order to optimize the model performance for transonic flows and through transition.

The Turbulence Model

The new Baseline (BSL) Model

The idea behind the BSL model is to retain the robust and accurate formulation of the Wilcox $k-\omega$ model in the near wall region, and to take advantage of the freestream independence of the $k-\epsilon$ model in the outer part of the boundary-layer. In order to achieve this, the $k-\epsilon$ model is transformed into a $k-\omega$ formulation. The difference between this formulation and the original $k-\omega$ model is that an additional cross-diffusion term appears in the ω-equation and that the modeling constants are different. The original model is then multiplied by a function F_1 and the transformed model by a function $(1-F_1)$ and both are added together. The function F_1 will be designed to be one in the near wall region (activating the original model) and zero away from the surface. The blending will take place in the wake region of the boundary-layer. The left hand side of the following equations is the Lagrangian derivative: $D/Dt := \partial/\partial t + u_i \partial/\partial x_i$.

Original $k-\omega$ model:

$$\frac{D\rho k}{Dt} = \tau_{ij}\frac{\partial u_i}{\partial x_j} - \beta^*\rho\omega k + \frac{\partial}{\partial x_j}\left[(\mu+\sigma_{k1}\mu_t)\frac{\partial k}{\partial x_j}\right] \quad (1)$$

$$\frac{D\rho\omega}{Dt} = \frac{\gamma_1}{\nu_t}\tau_{ij}\frac{\partial u_i}{\partial x_j} - \beta_1\rho\omega^2 + \frac{\partial}{\partial x_j}\left[(\mu+\sigma_{\omega 1}\mu_t)\frac{\partial \omega}{\partial x_j}\right] \quad (2)$$

Transformed $k-\epsilon$ model:

$$\frac{D\rho k}{Dt} = \tau_{ij}\frac{\partial u_i}{\partial x_j} - \beta^*\rho\omega k + \frac{\partial}{\partial x_j}\left[(\mu+\sigma_{k2}\mu_t)\frac{\partial k}{\partial x_j}\right] \quad (3)$$

$$\frac{D\rho\omega}{Dt} = \frac{\gamma_2}{\nu_t}\tau_{ij}\frac{\partial u_i}{\partial x_j} - \beta_2\rho\omega^2 + \frac{\partial}{\partial x_j}\left[(\mu+\sigma_{\omega 2}\mu_t)\frac{\partial \omega}{\partial x_j}\right] + 2\rho\sigma_{\omega 2}\frac{1}{\omega}\frac{\partial k}{\partial x_j}\frac{\partial \omega}{\partial x_j} \quad (4)$$

Now, equation (1) and equation (2) are multiplied by F_1 and equation (3) and equation (4) are multiplied by $(1-F_1)$ and the corresponding equations of each set are added together to give the new model:

$$\frac{D\rho k}{Dt} = \tau_{ij}\frac{\partial u_i}{\partial x_j} - \beta^*\rho\omega k + \frac{\partial}{\partial x_j}\left[(\mu+\sigma_k\mu_t)\frac{\partial k}{\partial x_j}\right] \quad (5)$$

$$\frac{D\rho\omega}{Dt} = \frac{\gamma}{\nu_t}\tau_{ij}\frac{\partial u_i}{\partial x_j} - \beta\rho\omega^2 + \frac{\partial}{\partial x_j}\left[(\mu+\sigma_\omega\mu_t)\frac{\partial \omega}{\partial x_j}\right] + 2\rho(1-F_1)\sigma_{\omega 2}\frac{1}{\omega}\frac{\partial k}{\partial x_j}\frac{\partial \omega}{\partial x_j}. \quad (6)$$

Let ϕ_1 represent any constant in the original model ($\sigma_{k1}, \ldots$), ϕ_2 any constant in the transformed $k-\epsilon$ model ($\sigma_{k2}, \ldots$) and ϕ the corresponding constant of the new model ($\sigma_k \ldots$), then the relation between them is:

$$\phi = F_1\phi_1 + (1-F_1)\phi_2. \quad (7)$$

the following two sets of constants will be used:

Set 1 (ϕ_1) (Wilcox):

$$\sigma_{k1} = 0.5, \sigma_{\omega 1} = 0.5, \beta_1 = 0.0750, \quad (8)$$
$$\beta^* = 0.09, \kappa = 0.41, \gamma_1 = \beta_1/\beta^* - \sigma_{\omega 1}\kappa^2/\sqrt{\beta^*}$$

Set 2 (ϕ_2) (standard $k-\epsilon$):

$$\sigma_{k2} = 1.0, \sigma_{\omega 2} = 0.856, \beta_2 = 0.0828, \quad (9)$$
$$\beta^* = 0.09, \quad \kappa = 0.41, \quad \gamma_2 = \beta_2/\beta^* - \sigma_{\omega 2}\kappa^2/\sqrt{\beta^*}.$$

Set 1 corresponds to the original $k-\omega$ model and will be used in the near wall region exclusively. Set 2 corresponds to the transformation of the standard $k-\epsilon$ model ($c_{1\epsilon} = 1.44, c_{2\epsilon} = 1.92$) and its main area of application is for free shear-layers.

The model has to be supplemented by the definition of the eddy-viscosity:

$$\nu_t =: \frac{\mu_t}{\rho} = \frac{k}{\omega}. \quad (10)$$

The turbulent stress tensor $\tau_{ij} = -\rho\overline{u_i' u_j'}$ is then given by:

$$\tau_{ij} = \mu_t\left(\frac{\partial u_i}{\partial x_j} + \frac{\partial u_j}{\partial x_i} - \frac{2}{3}\frac{\partial u_k}{\partial x_k}\delta_{ij}\right) - \frac{2}{3}\rho k\delta_{ij}. \quad (11)$$

In order to complete the derivation of the model it is necessary to define the blending function F_1. Starting from the surface, the function should be equal to one over a large portion of the boundary layer in order to preserve the desirable features of the $k-\omega$ model, but go to zero at the boundary layer edge to ensure the freestream independence

of the $k-\epsilon$ model. The function will be defined in terms of the variable:

$$arg_1 = min(max(\frac{\sqrt{k}}{0.09\omega y}; \frac{500\nu}{y^2\omega}); \frac{4\rho\sigma_{\omega 2}k}{CD_{k\omega}y^2}) \quad (12)$$

as follows:

$$F_1 = tanh(arg_1^4) \quad (13)$$

where $CD_{k\omega}$ is the cross-diffusion term of equation (4):

$$CD_{k\omega} = max(2\rho\sigma_{\omega 2}\frac{1}{\omega}\frac{\partial k}{\partial x_j}\frac{\partial \omega}{\partial x_j}, 10^{-20}) \quad (14)$$

The first argument in equation (12) is the turbulent length scale $L_t = \sqrt{k}/(0.09\omega)\,(= k^{3/2}/\epsilon)$, divided by the shortest distance to the next surface, y. The ratio L_t/y is equal to 2.5 in the logarithmic region of the boundary-layer and goes to zero towards the boundary-layer edge. The second argument in equation (12) ensures that the function F_1 does not go to zero in the viscous sublayer. The third argument is an additional safeguard against the "degenerate" solution of the original $k-\omega$ model with small freestream values for ω [13]. Figure 1a shows the typical behavior of the function F_1 for different velocity profiles in a strong adverse pressure gradient boundary layer (it also depicts the function F_2 explained later). Figure 1 also includes the underlying velocity profiles (same linestyle). The function is equal to one over about 50% of the boundary-layer and then gradually goes to zero. The behavior of the new BSL model will obviously lie somewhere between the original $k-\omega$ and the $k-\epsilon$ model. However, since most of the production of both, k and ω, takes place in the inner 50% of the layer, it can be expected that the model performance will be closer to that of the $k-\omega$ model, governing this area. Recall that the replacement of the ϵ equation by an algebraic length-scale, as proposed by [7, 8] has to be performed in the logarithmic region so that the original $k-\epsilon$ model still covers the largest part of the boundary layer and results will therefore be much closer to those of the $k-\epsilon$ model.

The Shear-Stress Transport (SST) Model

One of the major differences between eddy-viscosity and full Reynolds-stress models, with respect to aerodynamic applications, is that the latter accounts for the important effect of the transport of the principal turbulent shear-stress $\tau =: -\rho\overline{u'v'}$ (obvious notation) by the inclusion of the term

$$\frac{D\tau}{Dt} =: \frac{\partial \tau}{\partial t} + u_k\frac{\partial \tau}{\partial x_k}. \quad (15)$$

The importance of this term has clearly been demonstrated by the success of the Johnson-King (JK) [3] model. Note that the main difference between the JK - model and the Cebeci-Smith model lies in the inclusion of this term in the former, leading to significantly improved results for adverse pressure gradient flows. The JK model features a transport equation for the turbulent shear-stress τ that is based on Bradshaw's assumption that the shear-stress in a boundary-layer is proportional to the turbulent kinetic energy, k, :

$$\tau = \rho a_1 k \quad (16)$$

with a_1 being a constant. On the other hand, in two-equation models, the shear-stress is computed from:

$$\tau = \mu_t\Omega \quad (17)$$

with $\Omega = \frac{\partial u}{\partial y}$. For conventional two-equation models this relation can be rewritten to give:

$$\tau = \rho\sqrt{\frac{Production_k}{Dissipation_k}}a_1 k \quad (18)$$

as noted in [12]. In adverse pressure gradient flows the ratio of production to dissipation can be significantly larger than one, as found from the experimental data of Driver [15], and therefore equation (18) leads to an overprediction of τ. In order to satisfy equation (16) within the framework of an eddy-viscosity model, the eddy-viscosity would have to be redefined in the following way:

$$\nu_t = \frac{a_1 k}{\Omega}. \quad (19)$$

The rational behind this modification can also be explained in the following way: In conventional two-equation models the turbulent shear-stress responds instantaneously to changes in the shear-strain rate Ω, much like an algebraic eddy-viscosity model, whereas equation (19) guarantees that τ does not change more rapidly than $\rho a_1 k$. Obviously, equation (19) is not desirable for the complete flowfield, since it leads to infinitely high eddy-viscosities at points where Ω goes to zero. Note however, that in adverse pressure gradient flows, production is larger than dissipation for the largest part of the layer (or $\Omega > a_1\omega$). The following expression:

$$\nu_t = \frac{a_1 k}{max(a_1\omega; \Omega)} \quad (20)$$

guarantees therefore the selection of equation (19) for most of the adverse pressure gradient regions (wake region of the boundary layer), whereas the original equation (10) is used for the rest of the boundary layer. Figure 2 shows the relation of $(-\overline{u'v'}/a_1 k)$ versus $\sqrt{Production/Dissipation}$ for the SST model (equation (20)), the conventional $k-\omega$ ($k-\epsilon$) model (equation (10)), Bradshaw's relation (equation (16)) and a relation proposed by Coakley [10]. Note that Coakley's relation contains the relations of Bradshaw ($\beta = 1$) and that of the conventional two-equation models ($\beta = 0$) as a subset, but not equation (20) (β is a free parameter of Coakley's model).

In order to recover the original formulation of the eddy-viscosity for free shear-layers (where Bradshaws assumption, expressed in equation (16) does not necessarily hold)

the modification to the SST model has to be limited to wall bounded flows. This can be done in the same way as for the BSL model by applying a blending function F_2.

$$\nu_t = \frac{a_1 k}{max(a_1\omega; \Omega F_2)} \tag{21}$$

where F_2 is defined similarly to equation (13):

$$arg_2 = max(2\frac{\sqrt{k}}{0.09\omega y}; \frac{500\nu}{y^2\omega}) \tag{22}$$

$$F_2 = tanh(arg_2^2) \tag{23}$$

F_2 is depicted in Fig. 1b in the same way as F_1 in Fig. 1a. Since the modification to the eddy-viscosity has its largest impact in the wake region of the boundary layer, it is imperative that F_2 extends further out into the boundary-layer than F_1. (Note on the other hand that F_1 has to fall off to zero well within the boundary-layer in order to prevent the freestream dependence of the $k-\omega$ model).

This modification to the eddy-viscosity is used in connection with the BSL model derived above. However, in order to recover the correct behavior for a flat plate boundary layer, the diffusion constant σ_{k1} had to be adjusted accordingly. The constants for the SST model are:

Set 1 (SST - inner):

$$\sigma_{k1} = 0.85, \sigma_{\omega 1} = 0.5, \beta_1 = 0.0750, a_1 = 0.31, \tag{24}$$
$$\beta^* = 0.09, \ \kappa = 0.41, \ \gamma_1 = \beta_1/\beta^* - \sigma_{\omega 1}\kappa^2/\sqrt{\beta^*}.$$

Set 2 remains unchanged. Furthermore, for general flows Ω is taken to be the absolute value of the vorticity. Both models are given in their full form in Appendix A.

Two new turbulence models have been introduced in this section. Both can be regarded as zonal models, since they utilize different models for different areas of the flowfield. However, in contrast to the classical zonal approach the present models do not require an a priori knowledge of the flowfield in order to define the zonal boundaries where the different models are to be used. The change between the different sub-models is achieved by "smart" functions that can distinguish between the different zones. Note that similar functions could also be designed for the $k-\epsilon$ model. This makes it possible to design one set of constants for wall bounded flows and a second set for free shear-layers and to switch between the different sets in the same way as in equation (7).

The BSL model retains the advantages of the Wilcox $k-\omega$ model for boundary-layer applications, but avoids its undesirable freestream dependency. Furthermore it switches to the more accurate $k-\epsilon$ model for free shear-layer applications. In addition to this, the SST model modifies the definition of the eddy-viscosity for adverse pressure gradient boundary-layer flows in much the same way as the Johnson-King model does. From a computational point of view both models are not significantly more complex than the original $k-\omega$ model.

Boundary Conditions

At a no-slip wall, all turbulent quantities, except ω are set to zero. As pointed out by Wilcox [9], ω satisfies the following equation near the wall:

$$\omega \rightarrow \frac{6\nu}{\beta_1 y^2} \qquad \text{as} \qquad y \rightarrow 0. \tag{25}$$

Wilcox recommends to specify this analytical solution for the first few gridpoints away from the wall explicitly. The present author found it much easier and as accurate to implement the following boundary condition:

$$\omega = 10\frac{6\nu}{\beta_1(\Delta y)^2} \qquad \text{at} \qquad y = 0 \tag{26}$$

where Δy is the distance to the next point away from the wall. Equation (26) simulates the boundary condition 25 without the need of changing the solution at interior points. It should be noted that models based on the ω-equation give accurate results if the near wall values of ω are sufficiently large. Both, equations (25) and (26) satisfy this demand. The results are not sensitive to the factor (10) used in equation (26).

At inflow boundaries, the turbulence quantities are specified and at outflow boundaries a zero gradient is assumed.

Two of the computed flowfields have a rotational symmetry. In this case, the gradients of all turbulence quantities in the circumferential direction are set to zero.

Numerical Method

The mean flow equations are solved by the INS3D code of S. E. Rogers and D. Kwak [16] which is based on a pseudo-compressibility method. The convective terms are upwind differenced with a third-order flux-difference scheme. The viscous fluxes are differenced with second-order accurate central differences. The linear equations resulting from the first-order backward Euler time differencing are solved with an implicit line relaxation scheme.

The turbulence equations have been solved with a number of different schemes, from a third-order upwind differencing, to a second-order TVD (total variation diminishing) [17] to a first order upwind scheme. It was found in all computations that the solutions were virtually independent of the scheme used in the turbulence equations, although a change of accuracy in the mean flow solver had a large effect. The reason for the insensitivity to the treatment of the convection terms in the turbulence model is, that unlike in the Navier-Stokes equations, they are not the leading order

terms. For this reason most of the computations are based on a first order upwind scheme. The turbulence equations were solved decoupled from the mean flow equations in a separate subroutine. One of the important aspects in the discretization of turbulence models is the implicit treatment of the source terms. The following approximate linearization gave good numerical properties:

$$\frac{\partial}{\partial k}(P_k - D_k) \approx -\frac{D_k}{k} \tag{27}$$

$$\frac{\partial}{\partial \omega}(P_\omega + C_\omega - D_\omega) \approx -\frac{|C_\omega| + 2D_\omega}{\omega}. \tag{28}$$

where P, D, C are the production, the destruction and the additional cross diffusion terms respectively. The above expressions go to the left hand side of the algorithm with a change of sign and thereby increase the diagonal dominance of the method. The resulting numerical scheme has proven to be very robust and all of the computations with the $k-\omega$ models could be run with an infinite time step. An exception is the backward facing step flow where the time step had to be reduced for all models tested so far by the author. Furthermore, the computations could be started with very crude initial conditions (like freestream values).

Experience with two-equation turbulence models has shown that in regions of low values of ω (ϵ/k), small disturbances in the shear strain rate can lead to erroneous spikes in the eddy-viscosity in the freestream or near the boundary layer edge. In order to understand the effect, the transport equation for the eddy-viscosity was derived from the $k-\omega$ model for incompressible flows (note that $D\nu_t/Dt = 1/\omega Dk/Dt - k/\omega^2 D\omega/Dt$):

$$\frac{D\nu_t}{Dt} = (1-\gamma)\frac{\nu_t}{\omega}\left(\frac{\partial u_i}{\partial x_j} + \frac{\partial u_j}{\partial x_i}\right)\frac{\partial u_i}{\partial x_j} - (\beta^* - \beta)k + \ldots \tag{29}$$

If ω goes to zero and ν_t is finite (typically a fraction of the molecular viscosity), the production term for the eddy-vicosity goes to infinity for small disturbances in the strain rate. A simple way to prevent this from happening is to compute both the production term of k, P_k, and the dissipation term, D_k, and than to limit the production term by the following formula:

$$\tilde{P}_k = min(P_k, 20 \cdot D_k). \tag{30}$$

This limiter has been very carefully tested and it was found that even for complex flows the ratio of P_k/D_k reaches maximum levels of only about two inside shear layers. Therefore, Equation (30) does not change the solution but only eliminates the occurrence of spikes in the eddy-viscosity due to numerical "wiggles" in the shear-strain tensor. It also eliminated the unphysical buildup of eddy-viscosity in the stagnation region of an airfoil, as reported in [14]. Note that this is not a specific problem of the $k-\omega$ model but has also been observed with the $k-\epsilon$ model.

All computations have been performed on different grids, to ensure that the presented solutions are grid independent. The airfoil computations were performed on a standard grid kindly provided by S. E. Rogers [18].

Results

Flat Plate Boundary Layer

In order to show the motivation for the derivation of the BSL model, flat plate zero pressure gradient boundary-layer computations with different freestream values for ω have been performed. It has been shown in [13] that the correct freestream values for ω outside the boundary-layer are:

$$\omega_f = \frac{4}{\sqrt{\beta^*}}\frac{u_\tau^2}{U_e \delta^*}. \tag{31}$$

where $u_\tau = \sqrt{\tau_w/\rho}$ is the friction velocity, defined in terms of the wall shear-stress τ_w, U_e is the freestream velocity and δ^* is the displacement thickness. For the first set of computations, the above value has been specified at the inflow boundary in the freestream for both the original and the BSL $k-\omega$ model. Then, the above value was reduced by four orders of magnitude and the computations were repeated with both models. Note that the freestream value of k was also reduced in order to keep the freestream value of the eddy-viscosity constant (equal to the molecular viscosity). Figure 3 shows eddy-viscosity profiles for the original and the BSL $k-\omega$ model. The eddy-viscosity of the original model changes by almost 100% due to the changes in ω_f, whereas the BSL model gives the same results for both cases. The strong sensitivity of the original model to ω_f is clearly unacceptable and can lead to a severe deterioration of the results for complex flows, as will be shown later. Results of the SST model were also found to be independent of ω_f.

In each of the following comparisons between the different models, ω_f for the original $k-\omega$ model was always chosen according to equation (31) whenever possible. In cases where the freestream values had to be chosen differently, it will be mentioned in the text. Figure 4 shows a comparison of the SST, the BSL, the original $k-\omega$ and the Jones-Launder (JL) $k-\epsilon$ model (all JL model computations have been performed with damping functions as given in [19]) for a zero pressure gradient flat plate boundary layer. Obviously, all models predict the correct c_f-distributions and velocity profiles. The $k-\omega$ models can be run with the first gridpoint as far out as $y^+ = 3$ without a deterioration of the results.

Free Shear Layers

For free shear layers the SST and the BSL model reduce to the same model ($F_1 = 0; F_2 = 0$), which will be called new $k-\omega$ model in this subsection. Note that the new $k-\omega$ model is formally almost identical to the Jones-Launder $k-\epsilon$ model. However a small cross-diffusion term has

been neglected in the derivation of equation (4). In order to show that this term is truly negligible, the original $k-\epsilon$ model is also included in the comparison. All computations were performed with 200 gridpoints across the layer. A grid refinement study on a grid with 300 points gave the same results.

Figure 5 shows the results of the solution of the equilibrium far wake equations for the different models. The results are compared to the experimental data of Fage and Falkner [20]. Obviously, the new $k-\omega$ model and the JL $k-\epsilon$ model produce almost identical results. The original $k-\omega$ model predicts a somewhat lower spreading-rate than the other models. As is well known for two-equation models, they fail to predict the smooth behavior of the data at the edge of the layer. The freestream value for the original $k-\omega$ model has been derived from an expression similar to equation (31) [13].

Figure 6 shows solutions for a self-similar plane jet, as reported in [21]. Again, the new $k-\omega$ and the JL model produce almost identical results and are in very good agreement with the experiments, whereas the original $k-\omega$ model shows a rather peculiar behavior. A major difference between the far-wake flow and the present flow is that the freestream velocity is zero (still air). The only acceptable freestream value for ω in still air is $\omega_f = 0$, as can be seen from the equilibrium equations [13] and from physical intuition. The specification of small values for ω_f leads to large eddy-viscosities in the original $k-\omega$ model, as demonstrated in Fig. 3 for the flat plate boundary-layer. The same is true in the present flow to an even larger extent, because of the missing wall influence. The original $k-\omega$ model predicts about five times as high an eddy-viscosity as the other two models, resulting in the large spreading rates shown in Fig. 6.

A comparison with the free mixing-layer experiment of Liepman and Laufer [22] is shown in Fig. 7. Note that the freestream velocity below the mixing-layer is zero, leading to the same problem with the original $k-\omega$ model as for the plane jet. The other two models again produce almost identical results in acceptable agreement with the experiments.

Adverse Pressure Gradient Flows

One of the most important aspects of a turbulence model for aerodynamic applications is its ability to accurately predict adverse pressure gradient boundary-layer flows. It is especially important that a model can predict the location of flow separation and the displacement effect associated with it. The reason is that the viscous-inviscid interaction has a strong influence on the overall pressure distribution and therefore on the performance of the aerodynamic body.

The most widely used test case to measure the performance of turbulence models under adverse pressure gradient conditions is the flow reported by Samuel and Joubert [23]. It is a flat plate boundary-layer, developing under an increasingly adverse pressure gradient. The upstream Reynolds number is $1.7 \cdot 10^6 m^{-1}$. The flow is retarded by the pressure gradient, but not separated.

Two different sets of computations have been performed. At first, the experimental pressure distribution was specified at the outer edge of the computational domain (opposite to the wall). Since this is not a very straightforward boundary condition for a Navier-Stokes method, a second set of computations was performed based on the specification of an inviscid external streamline. The inviscid streamline $y(x)_s$ is defined by the preservation of mass:

$$\dot{m} = \int_0^{y(x)_s} \rho u_{exp.}(x,y)dy = const. \qquad (32)$$

Note that the specification of a streamline does not mean that the displacement thickness is prescribed like in an inverse boundary-layer method. Both computations produced very similar results. The solutions shown here are for the prescribed streamline, which is thought to be the more consistent boundary condition from a numerical point of view. The eddy-viscosity at the inflow boundary was determined from the experimental shear-stress and velocity profiles, the turbulent kinetic energy k from the requirement $k = (-\overline{u'v'})/a_1$ and ω and ϵ from the definition of the eddy-viscosity. The same grid of 90x90 points as in [12] was used for the computations. The results are virtually identical to those on a 60x60 and a 120x120 grid.

Figure 8 shows a comparison of the computed and the experimental skin-friction distribution. All three $k-\omega$ models reproduce the experimental data almost exactly, whereas the JL $k-\epsilon$ model gives significantly to high values.

Figure 9 shows the same comparison for the velocity profiles. There are no large differences to be found between the different models. Only the SST model predicts a somewhat stronger retardation of the flow near the surface. The same behavior has been observed with the Johnson-King model in [12].

Turbulent shear-stress profiles are shown in Fig. 10. All models are slightly overpredicting the amount of shear-stress, with the SST model closest and the JL model furthest away from the data.

It is obvious that the small differences between the solutions, especially between the different $k-\omega$ models, do not allow final conclusions about the abilities of the models to predict adverse pressure gradient flows. It appears that the Samuel-Joubert flow does not pose a sufficiently strong challenge to the models to assess their potentials for this type of flows. The author has reached a similar conclusion in [12], where a solution of the Johnson-King (JK) model has shown, that the model did not significantly depart from its equilibrium formulation. It is therefore important to test models under more demanding conditions, with stronger adverse pressure gradients and possibly separation. The following flowfield, reported by Driver [15], has proven to be a

highly self-consistent and demanding test case, and is therefore strongly recommended for the assessment of turbulence models under adverse pressure gradients.

In Driver's flow, a turbulent boundary-layer develops in the axial direction of a circular cylinder. An adverse pressure gradient is imposed by diverging wind tunnel walls and suction applied at these walls. The pressure gradient is strong enough to cause the flowfield to separate. The inflow Reynolds number is $2.8 \cdot 10^5$ based on the diameter D of the cylinder (140mm).

The boundary conditions for this flow are similar to those used for the Samuel-Joubert flow. Again an inviscid streamline is extracted from the experimental velocity profiles and a slip condition is applied along this line. The inflow conditions are determined from the experimental profiles in the same way as described above. The computations have been performed with a three-dimensional version of the code. In order to account for the axial symmetry, three closely spaced circumferential planes where introduced and symmetry conditions were applied. A 60x3x60 grid [12] was used for the present computations. A computation on a 100x3x100 grid gave almost identical results.

Figure 11 shows the wall pressure distribution for Driver's flow as computed by the different models. The SST model gives superior results to the other models due to its ability to account for the transport of the principal turbulent shear-stress. As expected, the JL $k-\epsilon$ model produces the worst results, and the BSL and the original $k-\omega$ model being close to each other in the middle.

Figure 12, depicting the wall shear-stress distribution for Driver's flow, shows that the SST model predicts the largest amount of separation, whereas the JL model stays firmly attached. Again, the BSL and the orig. $k-\omega$ model produce very similar results, in good agreement with the experiments.

The differences between the models can be seen more clearly in Fig. 13 which shows the velocity profiles. The SST model clearly produces the best agreement with the experiments. The larger displacement effect predicted by this model is reflected in the flattening of the c_p-distribution as observed in Fig. 11. The orig. $k-\omega$ model predicts slightly better results than the BSL model, and the JL $k-\epsilon$ model shows very little sensitivity to the pressure gradient, as already reflected in Figs. 11 and 12.

The reasons for the different behavior of the models can be seen in the following two pictures. Figure 14 compares turbulent shear-stress profiles at different stations. The experimental data are shown both, in a surface (Carth.) oriented and in a streamline (Strml.) oriented coordinate system. (Note that the numerical results were, due to the eddy-viscosity formulation, not found to be sensitive to small changes in direction).

The JL model obviously predicts significantly higher shear-stress levels than the other models, especially in the region where separation is approached. This in turn leads to the firmly attached velocity profiles of Fig. 13. The differences between the models can be seen more clearly by looking at the eddy-viscosity distributions. Figure 15 shows the maximum value of the kinematic eddy-viscosity profiles for all x-stations, nondimensionalized by $u_e\delta^*$. The SST model predicts the reduction of this quantity due to the adverse pressure gradient in very good agreement with the experiments. The BSL and the orig. $k-\omega$ model are very close to each other up to separation (around $x/D = 0$), whereas the orig. model is closer to the experiments in the recovery region. Both models give consistently to high values for the maximum eddy-viscosity in the adverse pressure gradient region. The $k-\epsilon$ model falls only barely below the value of 0.0168 recommended by Clauser for equilibrium boundary-layers (and used in the Cebeci-Smith model) and thereby fails to account for the nonequilibrium effects altogether.

Backward-Facing Step Flow

Results for the flow over a backward facing step as reported by Driver and Seegmiller [25] will be discussed next. This flowfield was a test case in the 1981 Stanford conference for the evaluation of turbulence models. However, most of the computations at the time were performed on comparatively coarse grids and there is substantial evidence that significantly finer grids have to be used in order to obtain grid-independent results [26]. The present computations have been performed on a 120x120 grid, with substantial grid refinement near the step. Figure 16 shows the distribution of gridpoints. As with the other flowfields a grid refinement study was made. The present results are virtually identical to those performed on a 90x90 and on a 240x240 grid. The Reynolds number, based on the upstream momentum thickness Θ is, $Re_\Theta = 5000$ and the ratio of the boundary-layer thickness to the step height is about 1.5. The expansion ratio (height of the tunnel behind the step divided by the height of the tunnel in front of the step) is 1.125.

Figure 17 shows a comparison of computed and experimental skin friction distributions. The $k-\omega$ models all perform significantly better than the $k-\epsilon$ model. The reattachment length of the four models are 6.4 (SST), 5.9 (BSL), 6.4 (org. $k-\omega$) and 5.5 (JL $k-\epsilon$) compared to a value of about 6.4 in the experiments. The reattachment length predicted by the $k-\epsilon$ model is better than previously reported, certainly as a result of the fine grid employed in the present computations (see also [26]). However, the model predicts significantly too large variations of c_f in the recirculation and the reattachment region. The good results of the $k-\omega$ models show that it is not necessary to account for the anisotropy of the stress tensor, as suggested in [27], in order to get accurate results for the reattachment length.

The surface pressure distribution, shown in Fig. 18, reflects the trends already seen in c_f. The larger the separation

region predicted by the model the larger is the displacement effect of the boundary layer and the smaller is the pressure rise in the expansion region after the step.

Figure 19 shows a comparison of the velocity profiles. All models fail to capture the relaxation downstream of reattachment correctly. The results of [27] show that this is also true for more complex models which account for anisotropy effects.

NACA 4412 Airfoil Flow

The following set of computations is for the flow around a NACA 4412 airfoil at 13.87 degrees angle of attack. The Reynolds number with respect to the chord length is $Re = 1.52 \cdot 10^6$. Experimental data for this flow have been reported by Coles and Wadcock [28]. The grid for the computations consists of 241x61 points and was made available by S. Rogers [18]. It is similar to the one used in [29].

In the experiment the transition was fixed by transition strips at x/c of 0.023 and 0.1 for the upper and lower surface respectively. As reported in [29], if these locations are specified in the computations, a laminar separation bubble appears before the transition point on the upper surface of the airfoil. This separation bubble was not observed in the experiments which indicates that transition may take place already before the strip is reached. Computations have been performed with and without a specified transition location and differences between the computations are small. Results are given here for the case were transition was not specified, so that the models picked their own transition location. Transition takes place at a downstream station of $x/c \approx 0.006$ on the upper and $x/c \approx 0.06$ on the lower surface of the airfoil.

Figure 20 shows a comparison of the computed and the experimental velocity profiles at different streamwise stations. The results are similar to those for the separated case of Driver, Fig. 13. Again, the SST model predicts the displacement effect in very good agreement with the experiments. The BSL model is showing some response to the pressure gradient, and produces results similar to those reported in [29] for the Baldwin-Barth model. Another interesting result of this computation is that the original $k-\omega$ model predicts velocity profiles even further away from the experiments than the Jones-Launder $k-\epsilon$ model. The reason for the poor performance of the orig. $k-\omega$ model lies in its freestream dependency. In order to understand the problem, one has to look at the development of ω from the inflow boundary to the leading edge of the airfoil. In this inviscid region production and diffusion of ω are zero. The balance in the ω equation reduces therefore to:

$$U_s \frac{d\omega}{ds} = -\beta\omega^2 \tag{33}$$

where s is the streamline direction and U_s is the velocity in this direction. Assuming that U_s is constant and equal to U_∞, the equation can be solved to give:

$$\omega(s) = \frac{1}{\frac{\beta}{U_\infty} s + \frac{1}{\omega_\infty}}. \tag{34}$$

The largest value of ω that can be achieved for a certain distance s from the inflow boundary is:

$$\omega(s) = \frac{1}{\frac{\beta}{U_\infty} s} \tag{35}$$

corresponding to an infinitely large ω_∞. As s gets large this maximum value becomes small. In the present computations, the distance between the inflow boundary and the airfoil is about 15 chord lengths. Non-dimensionalizing all quantities with U_∞ and the chord length, c, leads to a freestream value of ω in the leading edge region of the airfoil of about $\omega_f = 1$ whereas the formula given in [13] for the estimation of the correct freestream value:

$$\omega_f = \frac{u_\tau^2}{\sqrt{\beta} U_e \delta^*} 4 \tag{36}$$

indicates that it should be about three orders of magnitude larger. The low freestream value of ω in turn leads to the very high eddy-viscosities shown in Fig. 3 which in turn prevent separation. This example clearly shows the dangers of using the orig. $k-\omega$ model for aerodynamic applications. If the correct freestream values could be specified, the results of the orig. $k-\omega$ should be very close to those of the BSL model.

Figure 21 shows a comparison of the computed and the experimental surface pressure distributions. The agreement, especially for the SST model is not as good as should be expected from the velocity profiles shown in Fig. 20. Although the SST model predicts the displacement effect of the boundary layer almost exactly, it fails to reproduce the pressure distribution. This indicates an inconsistency between the computations and the experiments. Likely candidates are blockage effects in the wind tunnel (however, including wind tunnel walls in the computations does not improve the results [18]) or three-dimensional effects in the experiment.

Transonic Bump Flow

The final test case is the axisymmetric transonic shock-wave/turbulent boundary layer experiment of Bachalo and Johnson [30]. In this experiment, an axisymmetric boundary layer interacts with a shock wave created by a circular arc, as shown in Fig. 22. It is beyond the scope of this paper to present a detailed study of transonic flows and only the highest Mach number case will be shown. The Mach number for this experiment is 0.925. The number of gridpoints used was 150x3x80. Grid-independence was established by using different grids (129x3x60 and 180x3x100). Figure 23 shows the wall pressure distribution computed by the three different $k-\omega$ models, compared with the experiment. The

SST model predicts significantly better results than the BSL and the original $k-\omega$ model, due to its improved transport features. A compressible version of the $k-\epsilon$ model has not yet been coded and results for that model are therefore missing in the comparison. Earlier results of [31] show however a similar behavior as the BSL and the original $k-\omega$ model. Detailed comparisons for transonic flows will be presented at a later time.

Conclusions

Two new turbulence models have been derived from the original $k-\omega$ model of Wilcox [9]. The motivation behind the new baseline (BSL) model was to eliminate the freestream dependency of the $k-\omega$ model but retain its simple and reliable form, especially in the near wall region. In order to achieve this goal, a switching function was designed that can discriminate between the inner part (appr. 50%) of a boundary-layer and the rest of the flowfield. In this inner part the original $k-\omega$ model is solved, and in the outer wake region a gradual switch to the standard $k-\epsilon$ model, in a $k-\omega$ formulation, is performed.

The BSL model was then used to derive a model that can account for the transport of the turbulent shear stress (Shear-Stress Transport or SST model). The derivation of the model was inspired by the success of the Johnson-King (JK) model. The main assumption in the JK model that the principal turbulent shear-stress is proportional to the turbulent kinetic energy was incorporated into the new SST model. This modification ensures that the principal turbulent shear-stress satisfies the same transport equation as the turbulent kinetic energy. It is designed to act only inside the boundary-layer in order to retain the $k-\epsilon$ model (transformed to a $k-\omega$ formulation) for free shear-layers.

Both models were applied to a selection of well documented research flows, that are meaningful for aerodynamic applications. The results of the computations were compared against solutions of the standard $k-\omega$ and the standard $k-\epsilon$ model, as well as against experimental data.

The free shear-layer computations have shown that the new models give results almost identical to those of the $k-\epsilon$ model. Another important aspect of those computations is that they show clearly the strong ambiguity in the results of the original $k-\omega$ model with respect to freestream values.

The central part of the comparisons is for the behavior of the models under adverse pressure gradient conditions. The computations of the Samuel-Joubert flow, as well as Driver's separated adverse pressure gradient flow show that the SST model gives highly accurate results for this type of problem. The BSL and the original $k-\omega$ model produce rather similar results, provided the correct freestream values are specified in the latter.

Computations were also performed for the backward facing step flow of Driver and Seegmiller [25]. A very fine grid was employed to ensure grid independence of the results. For this problem, the original $k-\omega$ and the SST model give very accurate results. They predict the reattachment length within the uncertainty of the measurements and give an accurate representation of the wall pressure distribution. The BSL model gives about 8% too small values for the reattachment length. These results are still very accurate, considering the notorious difficulties this flow poses to numerical assessment. All models fail to predict the relaxation of the velocity profiles downstream of the reattachment point correctly.

Computations for a NACA 4412 airfoil at an angle of attack near maximum lift condition confirm the findings of the adverse pressure gradient computations. The SST model predicts highly accurate velocity profiles, almost identical to those of the experiments. The BSL model has a smaller sensitivity to the adverse pressure gradient than the SST model and therefore predicts less retarded profiles. A very surprising result of the computations is that the original $k-\omega$ model gives even less accurate solutions than the Jones-Launder $k-\epsilon$ model. The reason for the failure of the model is again its freestream dependency. This computation clearly shows that the original $k-\omega$ model cannot be applied unambiguously for industrial applications.

The last set of computations is for a transonic shock-wave/turbulent boundary layer interaction. The accurate prediction of the shock location by the SST model shows that the good performance of this model for incompressible applications can be extended to transonic flows.

Appendix
The Baseline (BSL) Model

$$\frac{D\rho k}{Dt} = \tau_{ij}\frac{\partial u_i}{\partial x_j} - \beta^*\rho\omega k + \frac{\partial}{\partial x_j}\left[(\mu + \sigma_k\mu_t)\frac{\partial k}{\partial x_j}\right] \tag{A-1}$$

$$\frac{D\rho\omega}{Dt} = \frac{\gamma}{\nu_t}\tau_{ij}\frac{\partial u_i}{\partial x_j} - \beta\rho\omega^2 + \frac{\partial}{\partial x_j}\left[(\mu + \sigma_\omega\mu_t)\frac{\partial \omega}{\partial x_j}\right] + 2(1-F_1)\rho\sigma_{\omega 2}\frac{1}{\omega}\frac{\partial k}{\partial x_j}\frac{\partial \omega}{\partial x_j} \tag{A-2}$$

The constants ϕ of the new model are calculated from the constants, ϕ_1, ϕ_2, as follows:

$$\phi = F_1\phi_1 + (1-F_1)\phi_2. \tag{A-3}$$

The constants of Set 1 (ϕ_1) are (Wilcox):

$$\sigma_{k1} = 0.5, \sigma_{\omega 1} = 0.5, \beta_1 = 0.0750, \tag{A-4}$$

$$\beta^* = 0.09, \ \kappa = 0.41, \ \gamma_1 = \beta_1/\beta^* - \sigma_{\omega 1}\kappa^2/\sqrt{\beta^*}.$$

The constants of Set 2 (ϕ_2) are (standard $k-\epsilon$):

$$\sigma_{k2} = 1.0, \sigma_{\omega 2} = 0.856, \beta_2 = 0.0828, \quad \text{(A-5)}$$
$$\beta^* = 0.09, \quad \kappa = 0.41, \quad \gamma_2 = \beta_2/\beta^* - \sigma_{\omega 2}\kappa^2/\sqrt{\beta^*}.$$

The function F_1 is defined as follows:

$$F_1 = tanh(arg_1^4) \quad \text{(A-6)}$$

with:

$$arg_1 = min(max(\frac{\sqrt{k}}{0.09\omega y}; \frac{500\nu}{y^2\omega}); \frac{4\rho\sigma_{\omega 2}k}{CD_{k\omega}y^2}) \quad \text{(A-7)}$$

where y is the distance to the next surface and $CD_{k\omega}$ is the cross-diffusion term of equation (A-2):

$$CD_{k\omega} = max(2\rho\sigma_{\omega 2}\frac{1}{\omega}\frac{\partial k}{\partial x_j}\frac{\partial \omega}{\partial x_j}, 10^{-20}) \quad \text{(A-8)}$$

The eddy-viscosity is defined as:

$$\nu_t = \frac{k}{\omega} \quad \text{(A-9)}$$

and the turbulent stress tensor $\tau_{ij} = -\rho\overline{u_i' u_j'}$ is:

$$\tau_{ij} = \mu_t(\frac{\partial u_i}{\partial x_j} + \frac{\partial u_j}{\partial x_i} - \frac{2}{3}\frac{\partial u_k}{\partial x_k}\delta_{ij}) - \frac{2}{3}\rho k\delta_{ij}. \quad \text{(A-10)}$$

The following choice of freestream values is recommended:

$$\omega_\infty = (1 \rightarrow 10)\frac{U_\infty}{L} \quad \text{(A-11)}$$
$$\nu_{t\infty} = 10^{-3}\nu$$
$$k_\infty = \nu_{t\infty}\omega_\infty \quad \text{(A-12)}$$

where L is the approximate length of the computational domain.

Appendix
The Shear-Stress Transport (SST) Model

The SST model is identical to the above formulation, except that the constants, ϕ_1, have to be changed to:

Set 1 (SST - inner):

$$\sigma_{k1} = 0.85, \sigma_{\omega 1} = 0.5, \beta_1 = 0.0750, a_1 = 0.31 \quad \text{(A-13)}$$
$$\beta^* = 0.09, \kappa = 0.41, \gamma_1 = \beta_1/\beta^* - \sigma_{\omega 1}\kappa^2/\sqrt{\beta^*}$$

and the eddy-viscosity is defined as:

$$\nu_t = \frac{a_1 k}{max(a_1\omega; \Omega F_2)}. \quad \text{(A-14)}$$

where Ω is the absolute value of the vorticity. F_2 is given by:

$$F_2 = tanh(arg_2^2) \quad \text{(A-15)}$$

with:

$$arg_2 = max(2\frac{\sqrt{k}}{0.09\omega y}; \frac{500\nu}{y^2\omega}) \quad \text{(A-16)}$$

Important detail !:

In applying this model, it is important that the reader is aware of the following ambiguity in the formulation of the production term of ω for the SST model. The definition of the production term of ω is sometimes written as:

$$P_\omega = \gamma\frac{\omega}{k}\tau_{ij}\frac{\partial u_i}{\partial x_j} \quad \text{(A-17)}$$

which introduces the nondimensional group $\nu_t\frac{\omega}{k}$ in front of the strain rate tensor. In the original and in the BSL model this group is equal to one and the two formulations for P_ω are therefore identical. This is not the case for the SST model because of equation (A-14). The SST model has been calibrated with respect to equation (A-2) and equation (A-17) should therefore not be used.

Acknowledgement

The author wants to thank Dr. S. E. Rogers and Dr. J. Bardina for providing the mean flow solvers for the incompressible and the transonic computations respectively, as well as their assistance in implementing the turbulence models.

References

[1]Cebeci, T. and Smith, A. M., *Analysis of Turbulent Boundary Layers, Academic Press, New York, 1974.*

[2]Baldwin, B. S. and Lomax, H., *"Thin Layer Approximation and Algebraic Model for Separated Turbulent Flows," AIAA Paper 78-257, Jan. 1978.*

[3]Johnson, D. A. and King, L. S., *"A Mathematically Simple Turbulence Closure Model for Attached and Separated Turbulent Boundary Layers," AIAA Journal, Vol. 23, Nov. 1985, pp. 1684-1692.*

[4]Jones, W. P. and Launder B. E., *"The Calculation of Low-Reynolds-Number-Phenomena with a Two-Equation Model of Turbulence," Int. J. Heat Mass Transf., Vol. 16, 1973, pp. 1119-1130.*

[5]Kline, S. J., Cantwell, B. J., Lilley, G. M., eds., *"1980-1981 AFOSR-HTTM Stanford Conference on Complex Turbulent Flows. Comparison of Computation and Experiment," Stanford University, Stanford, CA, 1981.*

[6]Rodi, W. and Scheurer, G., *" Scrutinizing the $k-\epsilon$ Model Under Adverse Pressure Gradient Conditions," J. Fluids Eng., 108, 1986, pp. 174-179.*

[7]Chen, H., C. and Patel, V. C., *"Near-Wall Turbulence Models for Complex Flows Including Separation," AIAA Journal, Vol. 26, No. 6, 1988.*

[8]Rodi, W., *"Experience with Two-Layer Models Combining the $k-\epsilon$ Model with a One-Equation Model Near the Wall," AIAA Paper 91-0216, Jan. 1991.*

[9]Wilcox, D. C., *"Reassessment of the Scale-Determining Equation for Advanced Turbulence Models," AIAA Journal, Vol.26, Nov. 1988, pp.1299-1310.*

[10]Coakley, T. J., *"Turbulence Modeling Methods for the Compressible Navier-Stokes Equations," AIAA Paper 83-1693, July 1982.*

[11]Wilox, D. C. and Rubesin, M. W., *"Progress in Turbulence Modeling for Complex Flow Fields Including the Effect of Compressibility," NASA TP-1517, 1980.*

[12]Menter, F. R., *"Performance of Popular Turbulence Models for Attached and Separated Adverse Pressure Gradient Flows," AIAA Journal, Vol. 30, Aug. 1992, pp. 2066-2072*

[13]Menter, F. R., *"Influence of Freestream Values on $k-\omega$ Turbulence Model Predictions ," AIAA Journal, Vol. 30, No. 6, 1992*

[14]Menter, F. R., *"Improved Two-Equation $k-\omega$ Turbulence Models for Aerodynamic Flows," NASA Technical Memorandum 103975, Oct. 1992*

[15]Driver, D. M., *"Reynolds Shear Stress Measurements in a Separated Boundary Layer," AIAA Paper 91-1787, 1991.*

[16]Rogers, S. E. and Kwak, D., *"An Upwind Differencing Scheme for the Time-Accurate Incompressible Navier-Stokes Equations," AIAA Paper 88-2583, Williamsburg, VA, 1988*

[17]Yee, H. C., Warming, R. F. and Harten, A., *"Implicit Total Variation Diminishing (TVD) Schemes for Steady-State Calculations in Gas Dynamics," Journal of Comp. Physics, Vol. 57, 1985, pp.327-360.*

[18]Rogers, S. E. *personal communication*

[19]Launder, B. E. and Sharma, B. I., *"Application of the Energy-Dissipation Model of Turbulence to the Calculation of Flow near a Spinning Disk," Letters in Heat and Mass Transfer , Vol.1, 1974, pp. 131-138.*

[20]Fage, A. and Falkner, V. M., *in Taylor G. I., Proc. Roy. Soc. London 135, 685, 1932*

[21]Wygnansky, I. and Fiedler, H. E., *"The Two-Dimensional Mixing Region," J. Fluid Mech., Vol. 41, part 2, 1970, pp. 327-361.*

[22]Liepman, H. W. and Laufer, J., *"Investigation of Free Turbulent Mixing," NACA TN 1257.*

[23]Samuel, A. E. and Joubert, P. N., *"A Boundary Layer Developing in an Increasingly Adverse Pressure Gradient," J. Fluid Mech. Vol. 66, part 3, 1974, pp. 481-505.*

[24]Driver, D. M., *personal communication*

[25]Driver, D. M. and Seegmiller, H. L., *"Features of a Reattaching Turbulent Shear Layer in Divergent Channel Flow," AIAA Journal, Vol. 23, No. 2, 1985.*

[26]Thangam, S. and Speciale, C. G., *"Turbulent Separated Flow Past a Backward-Facing Step: A Critical Evaluation of Two-Equation Turbulence Models," ICASE Report No. 91-23, 1991*

[27]Abid, R., Speciale, C. G. and Thangam, S., *"Application of a New $k-\tau$ Model to Near Wall Turbulent Flows," AIAA Paper 91-0614, Jan. 1991.*

[28]Coles, D. and Wadock, A. J., *"Flying-Hot-Wire Study of Flow Past an NACA 4412 Airfoil at Maximum Lift," AIAA Journal, Vol. 17, No.4, 1979.*

[29]Rogers, S. E., Wiltberg, N. L. and Kwak, D., *"Efficient Simulation of Incompressible Viscous Flow Over Single and Multi-Element Airfoils," AIAA Paper 92-0405, Jan. 1992.*

[30]Bachalo, W. D. and Johnson, D. A., *"An Investigation of Transonic Turbulent Boundary Layer Separation Generated on an Axisymmetric Flow Model," AIAA Paper 79-1479, Williamsburg, Va, 1979.*

[31]Horstman, C. C. and Johnson, D. A., *"Prediction of Transonic Separated Flows," AIAA Journal, Vol. 22, No.7, pp. 1001-1003, July 1984.*

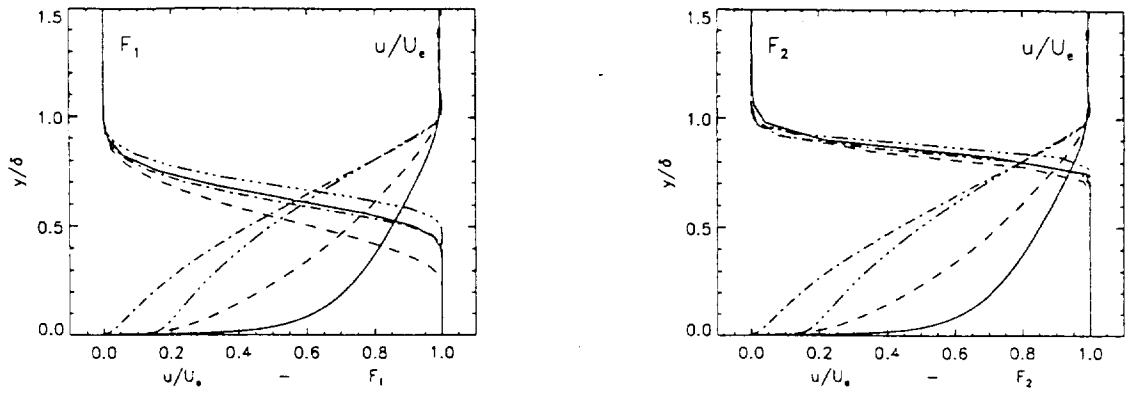

(a) Function F_1 (b) Function F_2

Fig. 1 Blending functions F_1 and F_2 versus y/δ for different velocity profiles.

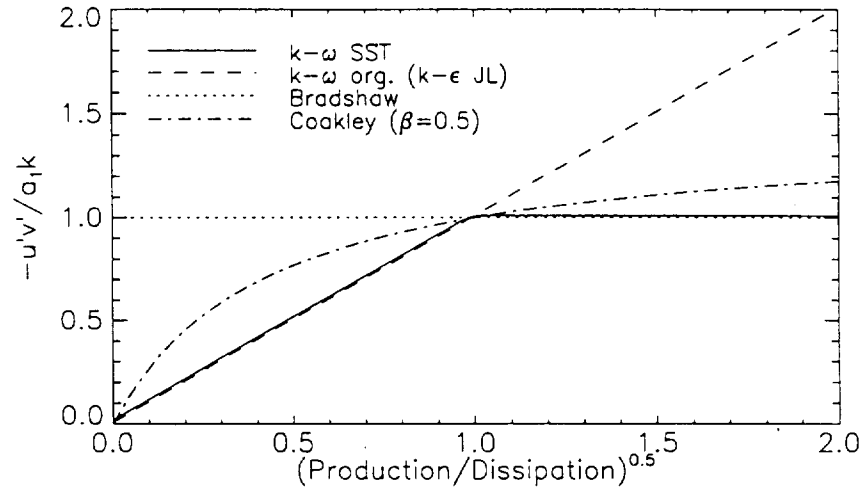

Fig. 2 Relation between $\frac{-\overline{u'v'}}{a_1 k}$ versus $\sqrt{\frac{Production}{Dissipation}}$ for different models.

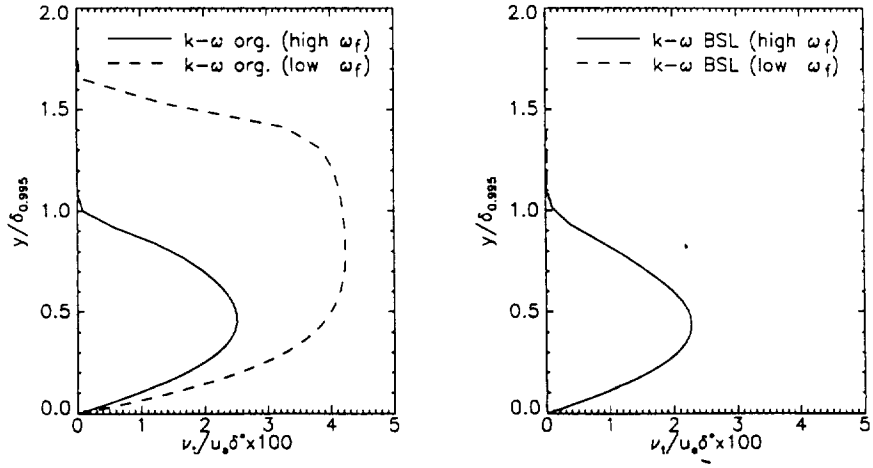

Fig. 3 Freestream-dependency of the eddy-viscosity for the original and the BSL $k-\omega$ model

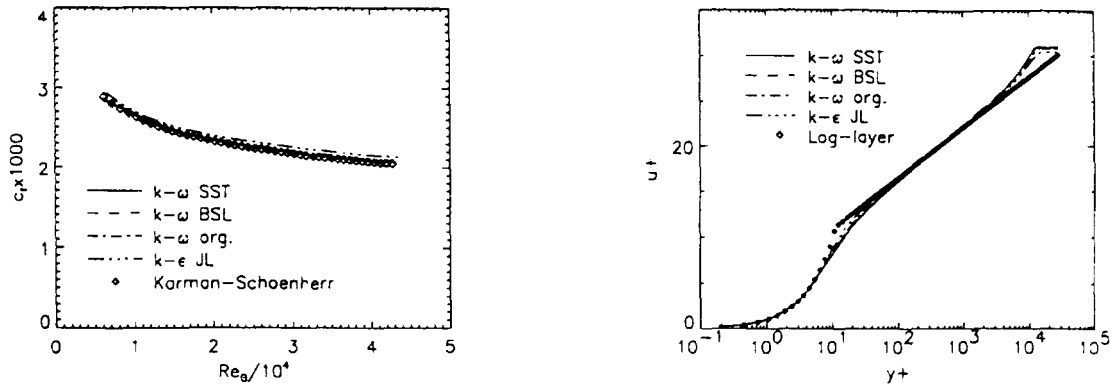

(a) Skin friction

(b) Law-of-the-wall

Fig. 4 Flat plate boundary-layer.

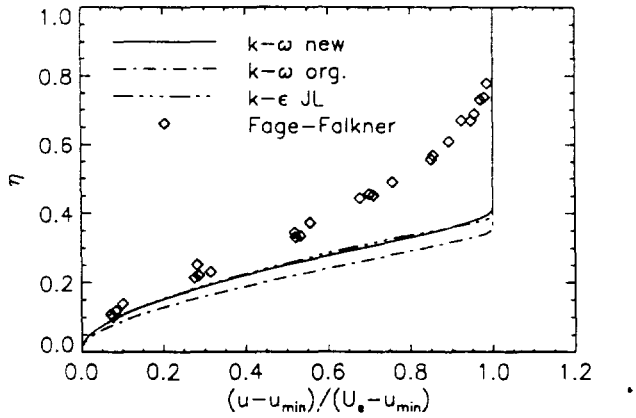

Fig. 5 Comparison of the velocity distribution of three different two-equation models for the far wake flow of Fage and Falkner

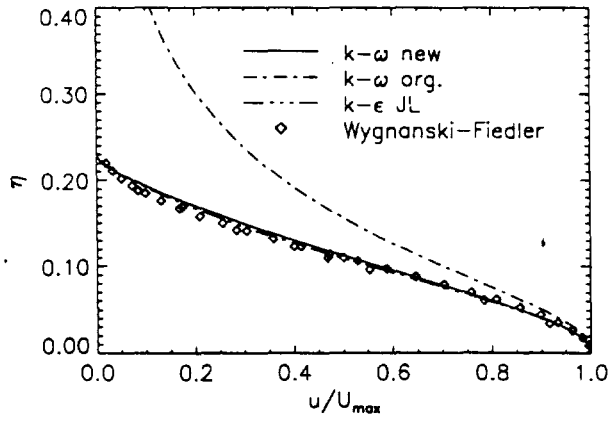

Fig. 6 Comparison of the velocity distribution of three different two-equation models for the plane jet flow of Wygnanski and Fiedler

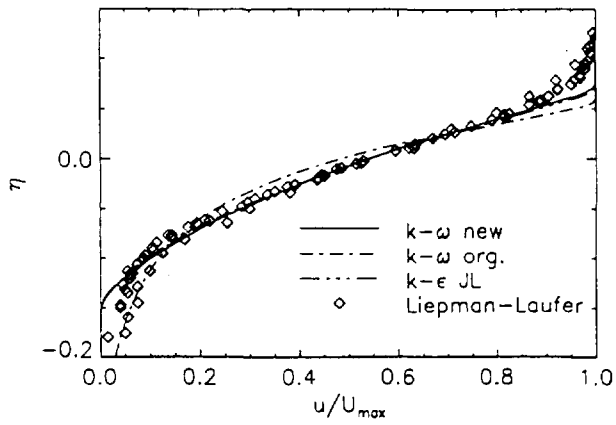

Fig. 7 Comparison of the velocity distribution of three different two-equation models for the free mixing-layer of Liepman and Laufer

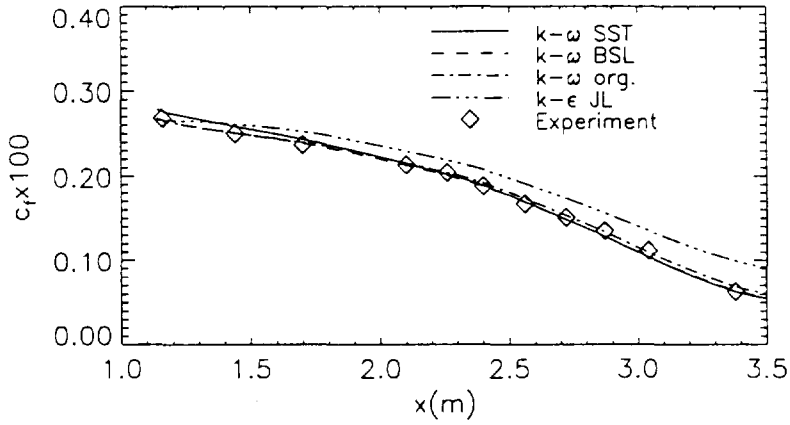

Fig. 8 Wall shear-stress distribution for Samuel-Joubert flow.

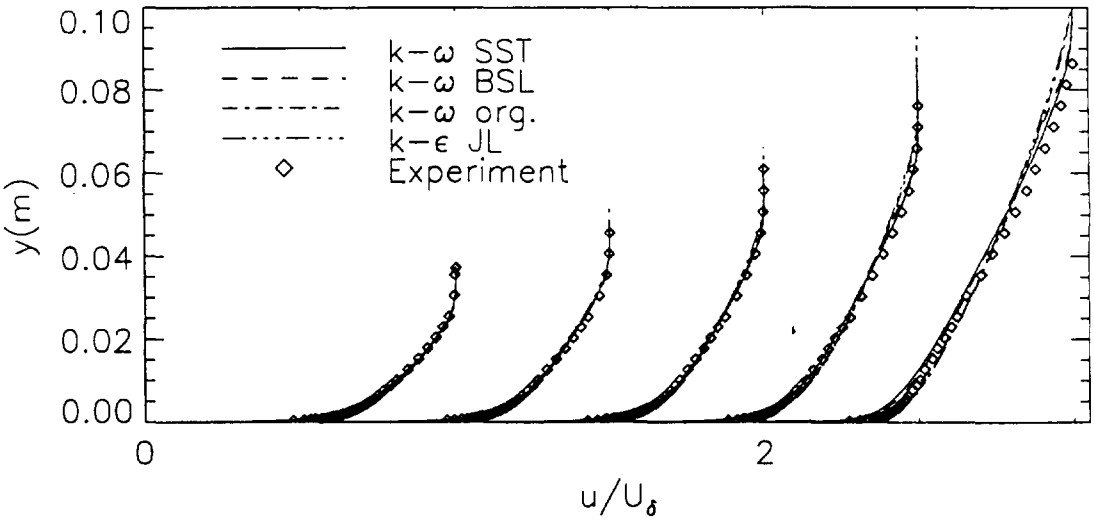

Fig. 9 Velocity profiles for Samuel-Joubert flow at x= 1.16, 1.76, 2.26, 2.87, 3.40 m.

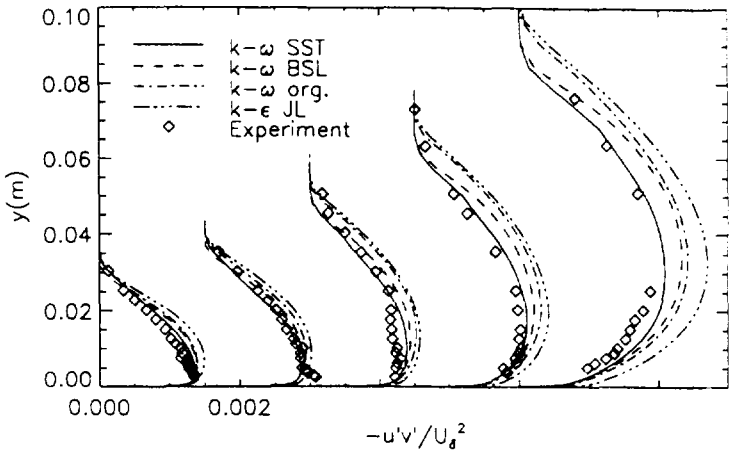

Fig. 10 Turbulent shear-stress profiles for Samuel-Joubert flow at x= 1.16, 1.76, 2.26, 2.87, 3.40 m.

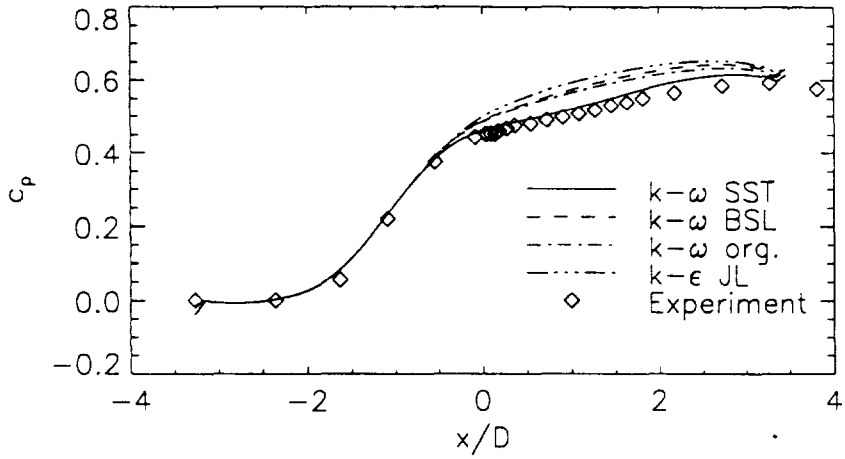

Fig. 11 Wall pressure distribution for Driver's adverse pressure-gradient flow.

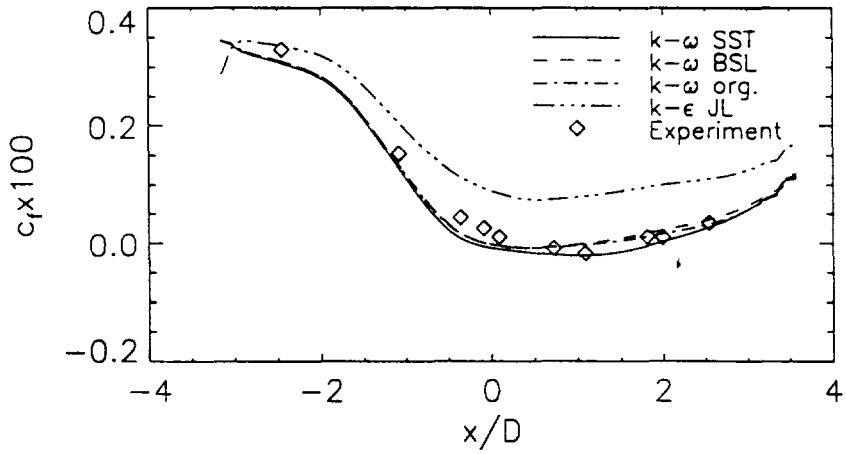

Fig. 12 Wall shear-stress distribution for Driver's adverse pressure-gradient flow.

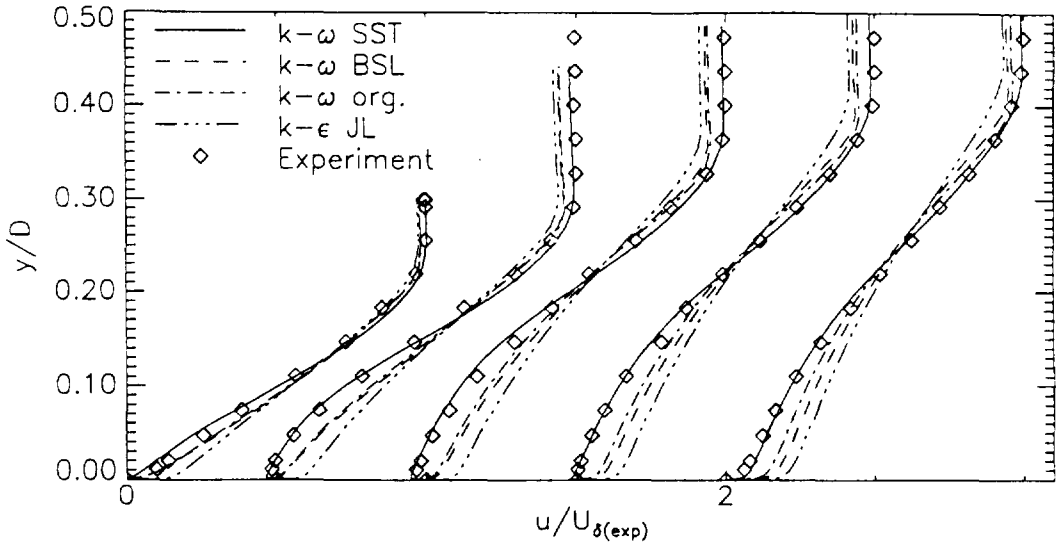

Fig. 13 Velocity profiles for Driver's adverse pressure-gradient flow at x/D=-0.091, 0.363, 1.088, 1.633, 2.177.

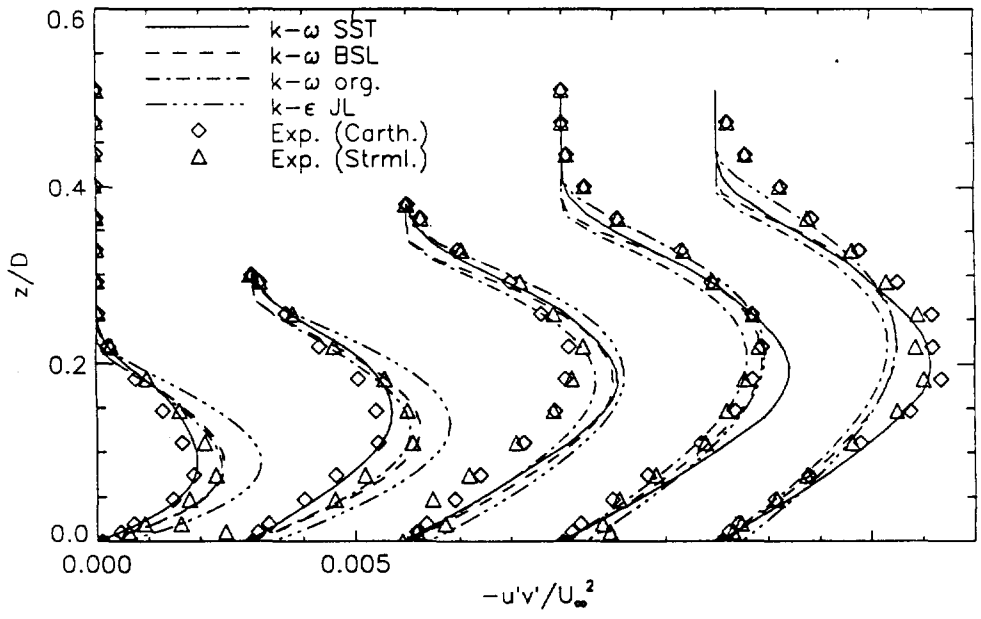

Fig. 14 Turbulent shear-stress profiles for Driver's adverse pressure-gradient flow at x/D=-0.091, 0.363, 1.088, 1.633, 2.177.

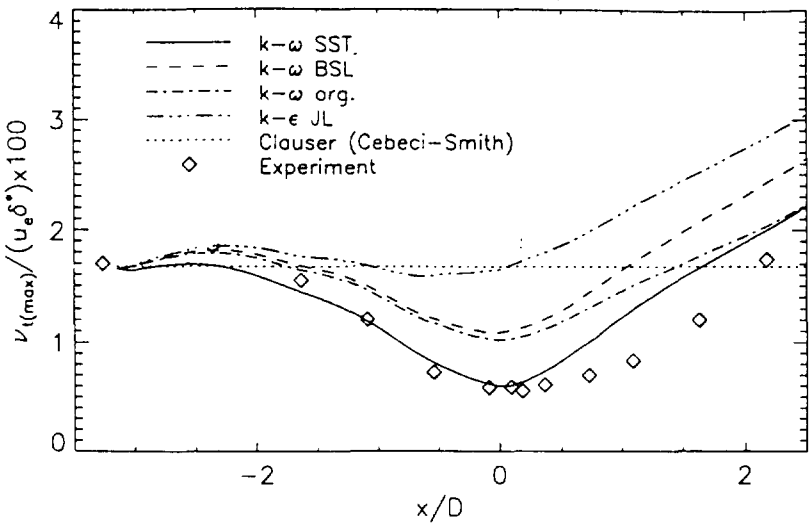

Fig. 15 $\frac{\nu_{t(max)}}{u_e\delta^*}$ distribution for Driver's adverse pressure-gradient flow.

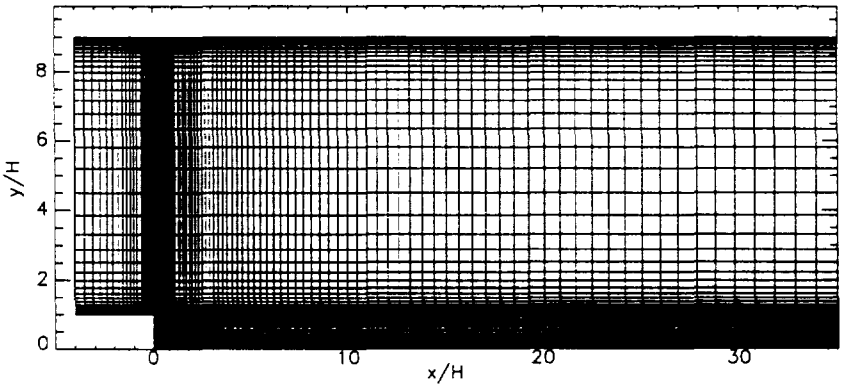

Fig. 16 Grid for backward-facing step (120x120 points).

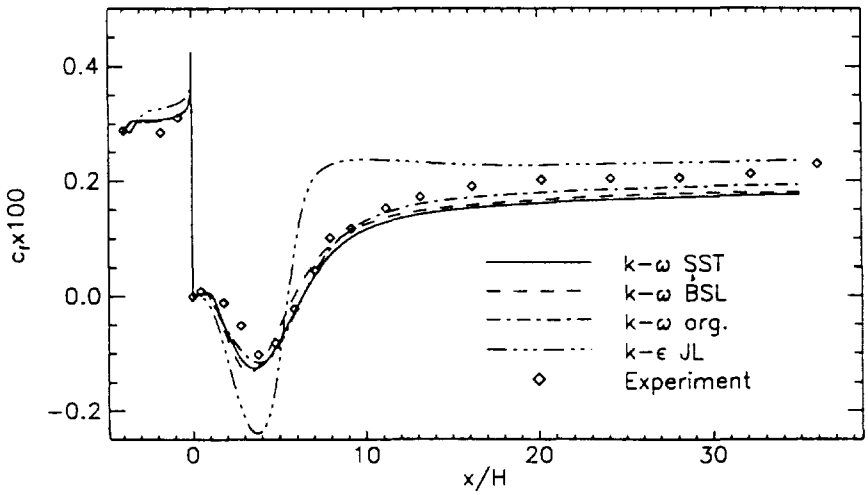

Fig. 17 Wall shear-stress distribution for backward-facing step flow.

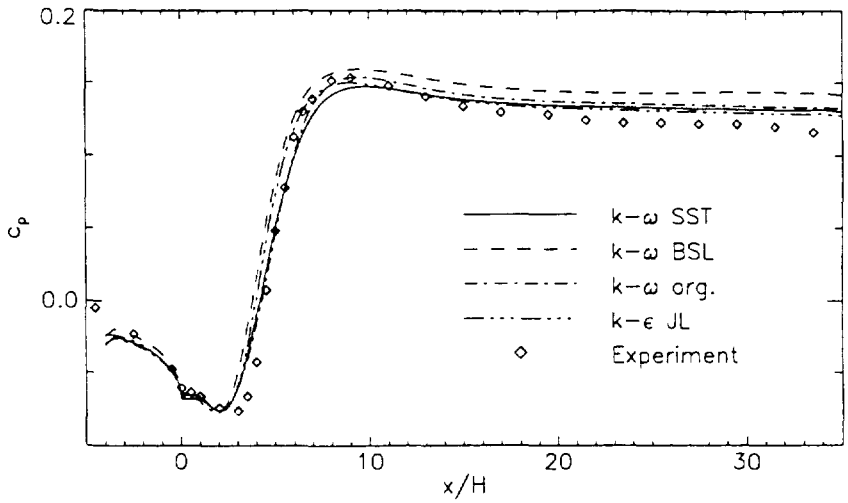

Fig. 18 Wall pressure distribution for backward-facing step flow.

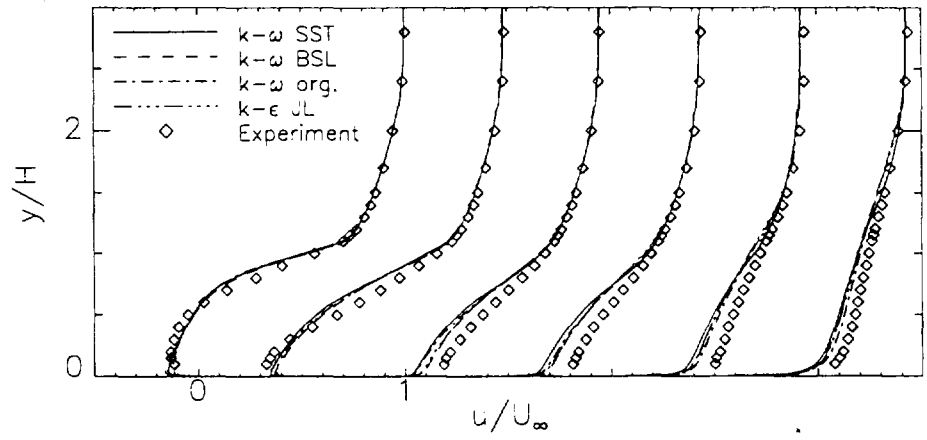

Fig. 19 Velocity profiles for backward-facing step flow at the streamwise locations: x/H= 2.0, 4.0, 6.5, 8.0, 14.0, 32.0.

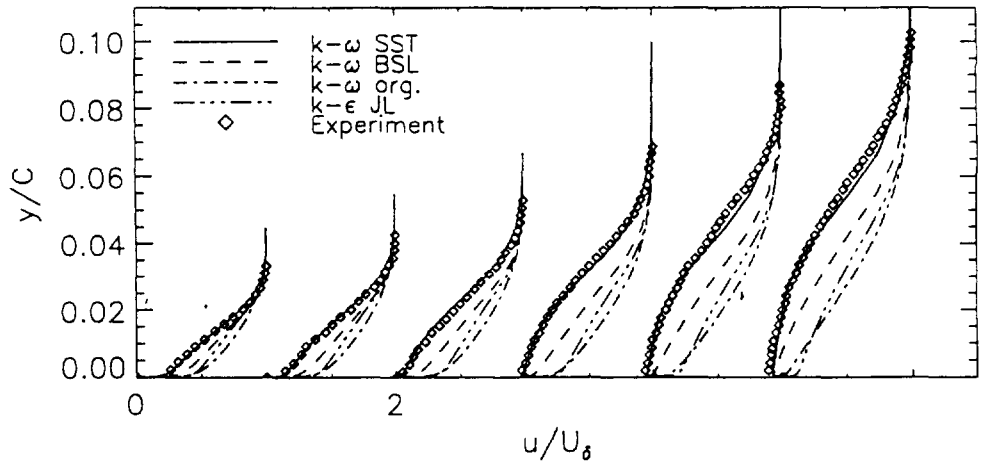

Fig. 20 Velocity profiles on the upper surface of a NACA 4412 airfoil at 13.87 degrees angle of attack. Streamwise stations x/c= 0.675, 0.731, 0.786, 0.842, 0.897, 0.953.

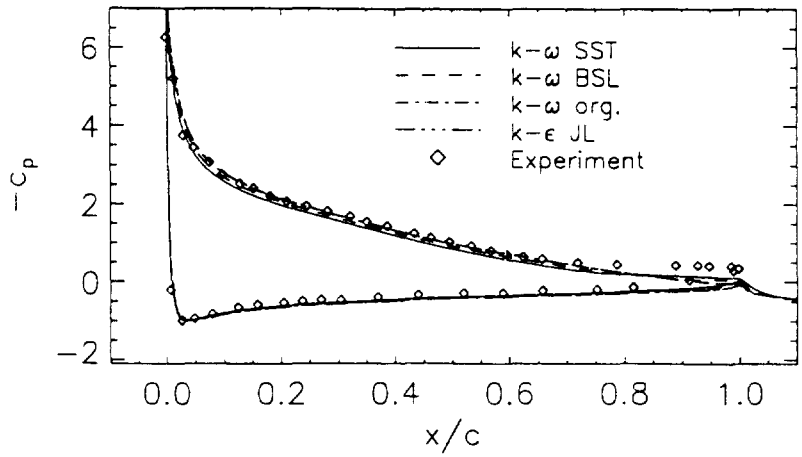

Fig. 21 Surface pressure distribution for a NACA 4412 airfoil at 13.87 degrees angle of attack.

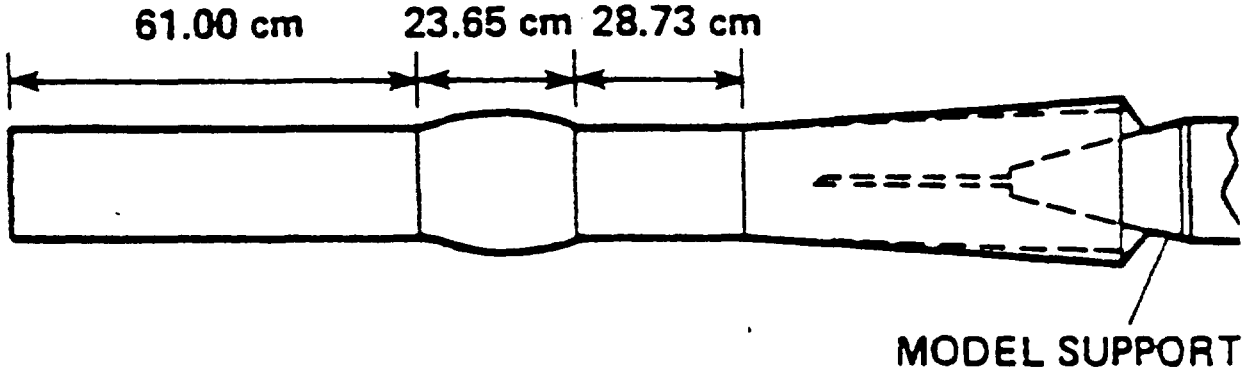

Fig. 22 Transonic bump flow experiment of Bachalo and Johnson

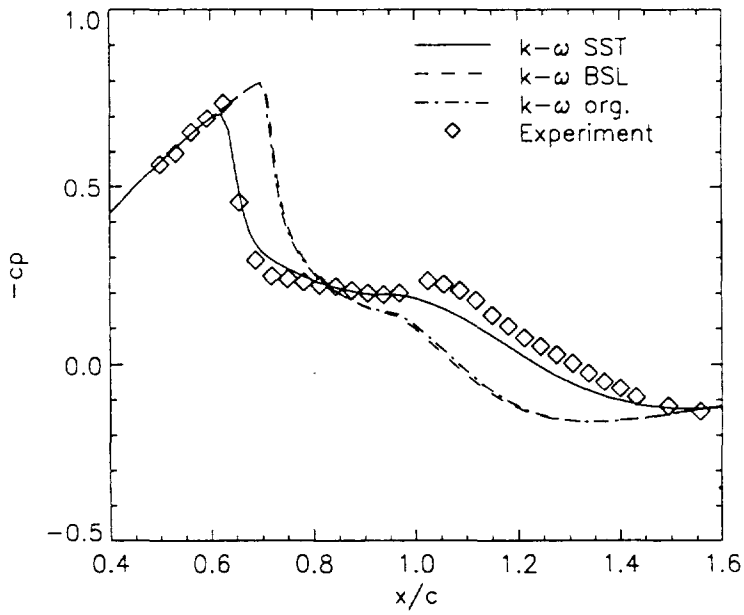

Fig. 23 Comparison of cp-distributions for transonic bump flow at M=0.925.